

# Low-dimensional chaos and wave turbulence in plasmas

BY A. M. BATISTA<sup>1,2</sup>, I. L. CALDAS<sup>2</sup>, S. R. LOPES<sup>3</sup> AND R. L. VIANA<sup>3,\*</sup>

<sup>1</sup>*Departamento de Matemática e Estatística, Universidade Estadual de Ponta Grossa, 84033-240 Ponta Grossa, Paraná, Brazil*

<sup>2</sup>*Instituto de Física, Universidade de São Paulo, Caixa Postal 66318, 05315-970 São Paulo, São Paulo, Brazil*

<sup>3</sup>*Departamento de Física, Universidade Federal do Paraná, Caixa Postal 19081, 81531-990 Curitiba, Paraná, Brazil*

We investigated drift-wave turbulence in the plasma edge of a small tokamak by considering solutions of the Hasegawa–Mima equation involving three interacting modes in Fourier space. The resulting low-dimensional dynamics presented periodic as well as chaotic evolution of the Fourier-mode amplitudes, and we performed the control of chaotic behaviour through the application of a fourth resonant wave of small amplitude.

**Keywords:** wave interaction; drift waves; wave turbulence

## 1. Introduction

Drift waves play an important role in the transport of energy and particles in magnetically confined plasmas, since the presence of steep density gradients in the plasma edge gives rise to turbulence, which can explain the anomalous transport rates observed experimentally (Horton 1999). A theoretical description of drift-wave propagation and the emergence of cross-field transport in tokamak plasmas has been proposed by Hasegawa & Mima (1977, 1978) leading to a partial differential equation for the electrostatic potential.

Solutions to the Hasegawa–Mima equation can be sought as Fourier-mode expansions, a procedure which yields an infinite number of coupled ordinary differential equations governing the time evolution of each mode amplitude (Horton & Hasegawa 1994). We performed a three-mode truncation of this system, analysing the dynamics of the resonant interacting modes, where we have added phenomenological growth/decay rates in order to include the energy injection in the triplet and its redistribution among the different modes interacting (Terry & Horton 1982, 1983). Energy transfer processes are key ingredients to explain the observed broadband spectrum of the drift-wave turbulence in the tokamak plasma edge (Wagner & Stroh 1993).

\* Author for correspondence (viana@fisica.ufpr.br).

One contribution of 14 to a Theme Issue ‘Experimental chaos II’.

The three waves have been chosen such that one is an energy pump mode and the other two are sidebands, a model which also arises in situations of interest in space plasma physics (Chian *et al.* 1994). The dynamics of the three-wave model has been analysed with special emphasis on the chaotic evolution of the complex Fourier-mode amplitudes found for wide ranges of the linear growth/decay rates. An intermittent route to chaos has previously been described for this kind of regime (Batista *et al.* 2006). In this paper we have focused on the possibility of controlling chaotic behaviour through the application of a fourth resonant mode with small amplitude. Our results are promising in view of the small amplitudes needed to stabilize chaotic wave dynamics into a low-period orbit.

This paper is organized as follows: in §2 we introduce the theoretical framework used to describe drift-wave turbulence, as well as the three-wave truncation model we deal with. In §3, the chaos control procedure is introduced. Our conclusions are left to §4.

## 2. Three-wave model

Drift waves in magnetically confined plasmas can be studied by means of the equation (Hasegawa & Mima 1977, 1978)

$$\frac{\partial}{\partial t}(\nabla^2\phi - \phi) - [(\nabla\phi \times \hat{z}) \cdot \nabla] \left[ \nabla^2\phi - \ln\left(\frac{n_0}{\omega_{ci}}\right) \right] = 0, \quad (2.1)$$

where  $\phi(\mathbf{x}, t)$  is the electrostatic potential;  $n_0$  is the background plasma density;  $\omega_{ci} = eB/m_i$  is the ion-cyclotron frequency;  $\mathbf{B} = B\hat{z}$  is the magnetic field; and  $e$  and  $m_i$  are the ion charge and mass, respectively. The operator  $\nabla$  stands for the gradient with respect to directions transverse to the magnetic field,  $\nabla = \hat{x}\partial/\partial x + \hat{y}\partial/\partial y$ . The rectangular geometry we use in our treatment is a large aspect-ratio approximation for the tokamak plasma edge, for which curvature effects are negligible in both toroidal and poloidal directions. In this case, the coordinates ( $x$ ,  $y$  and  $z$ ) stand for the radial position measured from the tokamak wall, the rectified poloidal and toroidal angles, respectively.

The Hasegawa–Mima equation can be derived from ion-fluid theory, assuming that the drift-wave frequency  $\omega$  is much smaller than  $\omega_{ci}$ , where the phase velocity along the magnetic field is such that  $v_{T_i} < (\omega/k_z) < v_{T_e}$ , where  $T_s$  is the thermal velocity for ions ( $s=i$ ) and electrons ( $s=e$ ) and  $(k_x, k_y, k_z)$  are the wavevector components. The drift-wave dispersion relation is (Horton & Hasegawa 1994)

$$\omega = \omega_{\mathbf{k}} = -\frac{1}{1+k^2} \left[ (\mathbf{k} \times \hat{z}) \cdot \nabla \ln\left(\frac{n_0}{\omega_{ci}}\right) \right]. \quad (2.2)$$

Drift waves have a characteristic dispersion scale length  $\rho_s = \sqrt{T_e/m_i}/\omega_{ci}$ , where  $T_e$  is the electron temperature, and which turns out to be the fundamental electric cross-field shielding distance for charge clumps in the regime of drift-wave fluctuations. In equation (2.1), the coordinates  $x$ ,  $y$ ,  $z$  have been rescaled by  $\rho_s$ , the time by  $\omega_{ci}$  and the potential by  $T_e/e$ .

We shall investigate numerical solutions of equation (2.1) through a Fourier-mode expansion of the electrostatic potential,

$$\phi(\mathbf{x}, t) = \frac{1}{2} \sum_{j=1}^{\infty} \left[ \phi_{\mathbf{k}_j}(t) \exp(i\mathbf{k}_j \cdot \mathbf{x}) + \phi_{\mathbf{k}_j}^*(t) \exp(-i\mathbf{k}_j \cdot \mathbf{x}) \right], \quad (2.3)$$

where  $\phi_{\mathbf{k}_j}(t)$  is a complex mode amplitude at a fixed position  $\mathbf{x}$ , corresponding to a wavevector  $\mathbf{k}_j$  and the asterisk stands for the complex conjugate. Substituting the expansion (2.3) into equation (2.1) yields an infinite system of coupled differential equations for the mode amplitudes (Katou 1982; Horton & Hasegawa 1994):

$$\frac{d\phi_{\mathbf{k}_j}}{dt} + i\omega_{\mathbf{k}_j} \phi_{\mathbf{k}_j} = \sum_{(\mathbf{k}_\alpha, \mathbf{k}_\beta, \mathbf{k}_\gamma)} A_{\mathbf{k}_\beta, \mathbf{k}_\gamma}^{\mathbf{k}_\alpha} \phi_{\mathbf{k}_\beta}^* \phi_{\mathbf{k}_\gamma}^*, \quad (2.4)$$

where  $j=1, 2, 3, \dots$ , and the summation runs over wavevector triplets which satisfy the resonant condition  $\mathbf{k}_\alpha + \mathbf{k}_\beta + \mathbf{k}_\gamma = 0$  for any choice of  $\mathbf{k}_j$ . The drift-wave mode frequencies are given by the dispersion relation (2.2), and the coupling coefficients are given by

$$A_{\mathbf{k}_\beta, \mathbf{k}_\gamma}^{\mathbf{k}_\alpha} = \frac{(\mathbf{k}_\gamma^2 - \mathbf{k}_\beta^2)}{2(1 + \mathbf{k}_\alpha^2)} (\mathbf{k}_\beta \times \mathbf{k}_\gamma) \cdot \hat{\mathbf{z}}. \quad (2.5)$$

In principle we would need a very large number of modes in order to describe a fully turbulent scenario due to the drift waves. However, we are chiefly interested to investigate the onset of turbulence, i.e. the scenario where a small number of modes becomes unstable, leading to a cascade of higher modes. Accordingly, in a lowest-order truncation of equation (2.4) we retained three resonant modes satisfying the resonance conditions

$$\mathbf{k}_1 + \mathbf{k}_2 + \mathbf{k}_3 = 0 \quad \text{and} \quad (2.6)$$

$$\omega_{\mathbf{k}_1} + \omega_{\mathbf{k}_2} + \omega_{\mathbf{k}_3} \approx 0. \quad (2.7)$$

Note that the second condition holds only in an approximate way, i.e. we allow for a (small) frequency mismatch. Moreover, the first condition can be thought of as defining a vector triangle in a  $z=\text{constant}$  plane transversal to the toroidal coordinate.

The three-mode system reads (Hasegawa *et al.* 1979)

$$\frac{d\phi_1}{dt} + i\omega_1 \phi_1 = A_{2,3}^1 \phi_2^* \phi_3^* + \gamma_1 \phi_1, \quad (2.8)$$

$$\frac{d\phi_2}{dt} + i\omega_2 \phi_2 = A_{3,1}^2 \phi_3^* \phi_1^* + \gamma_2 \phi_2 \quad \text{and} \quad (2.9)$$

$$\frac{d\phi_3}{dt} + i\omega_3 \phi_3 = A_{1,2}^3 \phi_1^* \phi_2^* + \gamma_3 \phi_3, \quad (2.10)$$

where we introduced the shorthand notation:  $\phi_j = \phi_{\mathbf{k}_j}$  and  $\omega_j = \omega_{\mathbf{k}_j}$ . We introduced phenomenological dissipative terms in the coupled mode equations to represent the energy injection necessary to sustain the wave interactions, where  $\gamma_i$  are growth/decay coefficients (Terry & Horton 1982, 1983).

In this paper we used typical parameter values of small tokamaks: toroidal magnetic field  $B=0.4$  T; electron temperature  $T_e=10$  eV; and electron density  $n_0=7\times 10^{18}$  m $^{-3}$ , from which we estimated the ion-cyclotron frequency to be  $3.82\times 10^7$  Hz and the length-scale is thus  $\rho_s\approx 10^{-3}$  m. The radial density gradient at the plasma edge was estimated, on the basis of particle flux measurements, to be (Heller *et al.* 1997)

$$\mathcal{N} := \rho_s \left| \nabla \ln \left( \frac{n_0}{\omega_{ci}} \right) \right| = \rho_s \left| \frac{\nabla n_0}{n_0} \right| \approx 0.17. \quad (2.11)$$

Measurements of potential edge fluctuations in small tokamaks give a poloidal wavenumber  $k_y$  in the range of  $(1-5)\times 10^3$  m $^{-1}$ , with a broad spectral content in the kHz range and a more pronounced peak at 50 kHz (Castro *et al.* 1996). The other wavevector components were estimated using linear relations and applying the resonance condition (2.6), such that the normalized frequencies can be chosen as  $|\omega_1| = \omega_2 = |\omega_3| = 1.31 \times 10^{-3}$ , and are related to the wavevectors through the dispersion relations (Batista *et al.* 2006)

$$\omega_i = \frac{(k_{iy} - k_{ix}^*)}{1 + k_i^2} \mathcal{N}, \quad (i = 1, 2, 3), \quad (2.12)$$

from which we can estimate the coupling coefficients in equations (3.3)–(3.5) as

$$A_{2,3}^1 = 32.8\omega_1 = 0.04, \quad (2.13)$$

$$A_{3,1}^2 = -421.8\omega_1 = -0.5 \quad \text{and} \quad (2.14)$$

$$A_{1,2}^3 = 335.9\omega_1 = 0.4. \quad (2.15)$$

Moreover, we shall assume that  $\phi_2$  is the inductor wave, which pumps energy to the daughter waves  $\phi_1$  and  $\phi_3$ ; and the values of their growth/decay coefficients are adjusted to the  $-50$  to  $+50$  V range for the floating electrostatic potential (Castro *et al.* 1996):  $\gamma_1 = \gamma_3 < 0$  and  $\gamma_2 = 0.01$ , the former rates being our tunable parameter.

Since the three Fourier modes retained  $\phi_i$  are complex variables, the phase space of the system has six dimensions. We can write them in exponential form as

$$\phi_1 = \sqrt{F_1} e^{i\varphi_1}, \quad (2.16)$$

$$\phi_2 = \sqrt{F_2} e^{i\varphi_2} \quad \text{and} \quad (2.17)$$

$$\phi_3 = \sqrt{F_3} e^{i\varphi_3}, \quad (2.18)$$

where  $\sqrt{F_i}$  and  $\phi_i$  are the real and imaginary parts of  $\phi_i$ ,  $i = 1, 2, 3$ . Substituting (2.16)–(2.18) into the three-mode equations (2.8)–(2.10), one obtains six real equations. For the mode  $\phi_1$ , the real and imaginary parts obey the equations

$$\dot{F}_1 = A_{2,3}^1 2\sqrt{F_1 F_2 F_3} \cos(\varphi_2 + \varphi_3 + \varphi_1) + \gamma F_1 \quad \text{and} \quad (2.19)$$

$$\dot{\varphi}_1 = -A_{2,3}^1 \sqrt{\frac{F_2 F_3}{F_1}} \sin(\varphi_2 + \varphi_3 + \varphi_1) - \omega_1 \quad (2.20)$$

and similar equations for the time evolution of  $F_2$ ,  $\phi_2$ ,  $F_3$  and  $\phi_3$ .

We can simplify the above system by defining the new angle (phase conjugacy)

$$\psi \equiv \varphi_2 + \varphi_3 + \varphi_1. \tag{2.21}$$

Dotting the above expression and substituting the corresponding equations for  $\phi_i$ , we eventually find an equation governing the time evolution of the new angle

$$\dot{\psi} = \mathcal{A} \sin \psi - \Delta\omega, \tag{2.22}$$

where the term  $\mathcal{A}$  depends on the coupling coefficients  $A_{i,j}^k$  and on the amplitudes  $\sqrt{F_i}$ ; and  $\Delta\omega = \omega_1 + \omega_2 + \omega_3$  is the non-zero frequency mismatch.

Hence, the original set of six equations can be reduced to just four equations, namely the three ones describing  $F_i$  plus equation (2.22) describing  $\dot{\psi}$ . Moreover, in all these equations, the phases appear combined in the same way, such that this phase conjugacy introduces a constraint in the six-dimensional phase space of the problem, and the trajectories must lie on a four-dimensional subset of the phase space. The resulting dynamical system makes phase-space volumes shrink with time with a constant rate given by  $2(\gamma_1 + \gamma_2 + \gamma_3) < 0$ , such that equations (2.8)–(2.10) are a globally dissipative dynamical system, whose dynamical behaviour can be conveniently investigated through two-dimensional projections and/or Poincaré maps.

### 3. Control of chaos

Once we have related electrostatic turbulent fluctuations to the low-dimensional chaotic behaviour of drift-wave modes, one may think of a control of chaos strategy with the purpose of reducing or suppressing weak turbulence. This intervention may control the chaotic time evolution in a given spatial scale, unless a collective effect sets in. Such a collective effect has been observed in some control strategies of spatially extended systems, where a pinning scheme consisting of localized perturbations in space has been successfully used (Hu & He 1993).

Our control strategy is based on the addition of a fourth resonant wave with small amplitude. Resonant four-wave coupling involves the interaction of two wave triplets. The presence of the second triplet having two waves in common with the first can either increase or stabilize the instability of the first triplet (Karplyuk *et al.* 1973; Walters & Lewak 1977). Accordingly, we introduced a new resonance into the system by including a fourth wave  $\phi_4$ , obeying the additional resonant conditions,

$$\mathbf{k}_4 = \mathbf{k}_1 + \mathbf{k}_2 \quad \text{and} \tag{3.1}$$

$$\omega_4 \approx \omega_1 + \omega_2. \tag{3.2}$$

The amplitude of the control wave is kept constant so that  $d\epsilon/dt = 0$  and small enough such that  $|\phi_4| \equiv \epsilon \ll |\phi_{1,2,3}|$  (Lopes & Chian 1996).

Retaining the fourth resonant wave in equation (2.4), there results the modified system

$$\frac{d\phi_1}{dt} + i\omega_1\phi_1 = A_{2,3}^1\phi_2^*\phi_3^* + \gamma_1\phi_1 + |\epsilon|\phi_2^*, \tag{3.3}$$

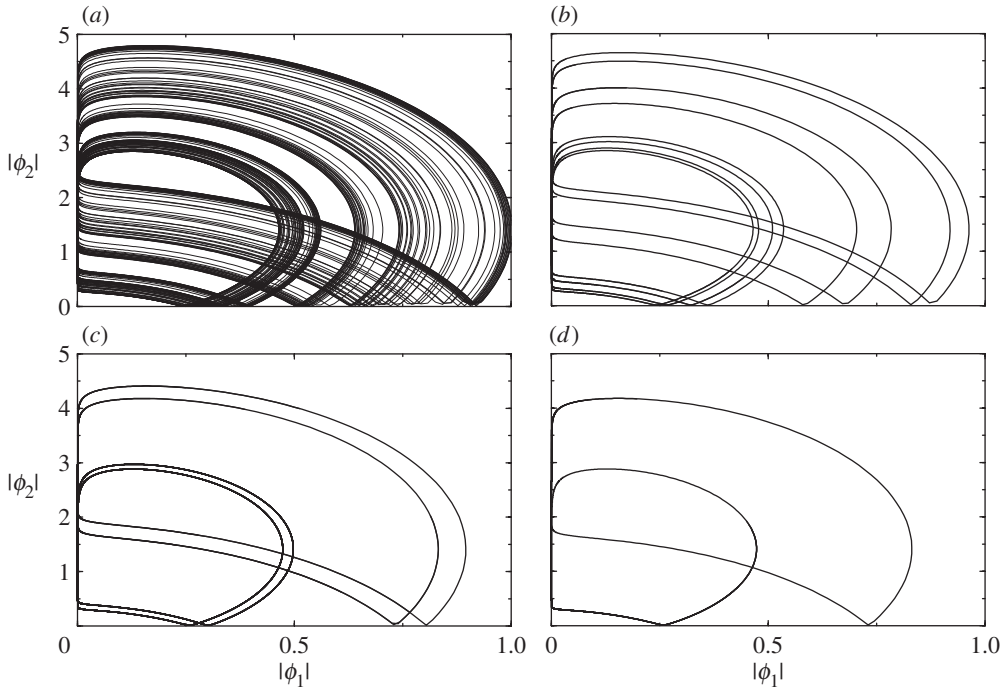


Figure 1. Projection of the phase space showing the attractors obtained for  $\gamma_2=0.01$ ,  $\gamma_1=\gamma_3=-0.194$  and (a)  $\epsilon=0$ , (b)  $\epsilon=10^{-12}$ , (c)  $\epsilon=10^{-11}$ , (d)  $\epsilon=10^{-10}$ .

$$\frac{d\phi_2}{dt} + i\omega_2\phi_2 = \Lambda_{3,1}^2\phi_3^*\phi_1^* + \gamma_2\phi_2 + |\epsilon|\phi_1^* \quad \text{and} \quad (3.4)$$

$$\frac{d\phi_3}{dt} + i\omega_3\phi_3 = \Lambda_{1,2}^3\phi_1^*\phi_2^* + \gamma_3\phi_3. \quad (3.5)$$

We integrated numerically equations (3.3)–(3.5) using a twelfth-order Adams method and the initial conditions,

$$\text{Re } \phi_1(0) = \text{Re } \phi_2(0) = \text{Re } \phi_3(0) = 0.1 \quad \text{and} \quad (3.6)$$

$$\text{Im } \phi_1(0) = \text{Im } \phi_1(0) = \text{Im } \phi_1(0) = 0.0. \quad (3.7)$$

A representative example of the control procedure is shown in figure 1. We set  $\gamma_1=-0.194$  and plotted two-dimensional projections of the four-dimensional subset of phase space to which the trajectories are constrained to stay, due to the phase conjugacy described at the end of §2. We used as coordinates the moduli of two of the waves, in plots of  $|\phi_1|$  versus  $|\phi_2|$ . Other choices of coordinates would produce similar results. We observe in figure 1a that the uncontrolled situation ( $\epsilon=0$ ) exhibits an apparently chaotic attractor in the phase projection chosen. The addition of a fourth wave, with an amplitude as small as  $\epsilon=10^{-12}$  is already enough to steer the phase-space trajectories into a period-eight orbit (figure 1b). Other orbits with periods equal to 4 and 2 can be obtained using  $\epsilon=10^{-11}$  (figure 1c) and  $10^{-10}$  (figure 1d), respectively.

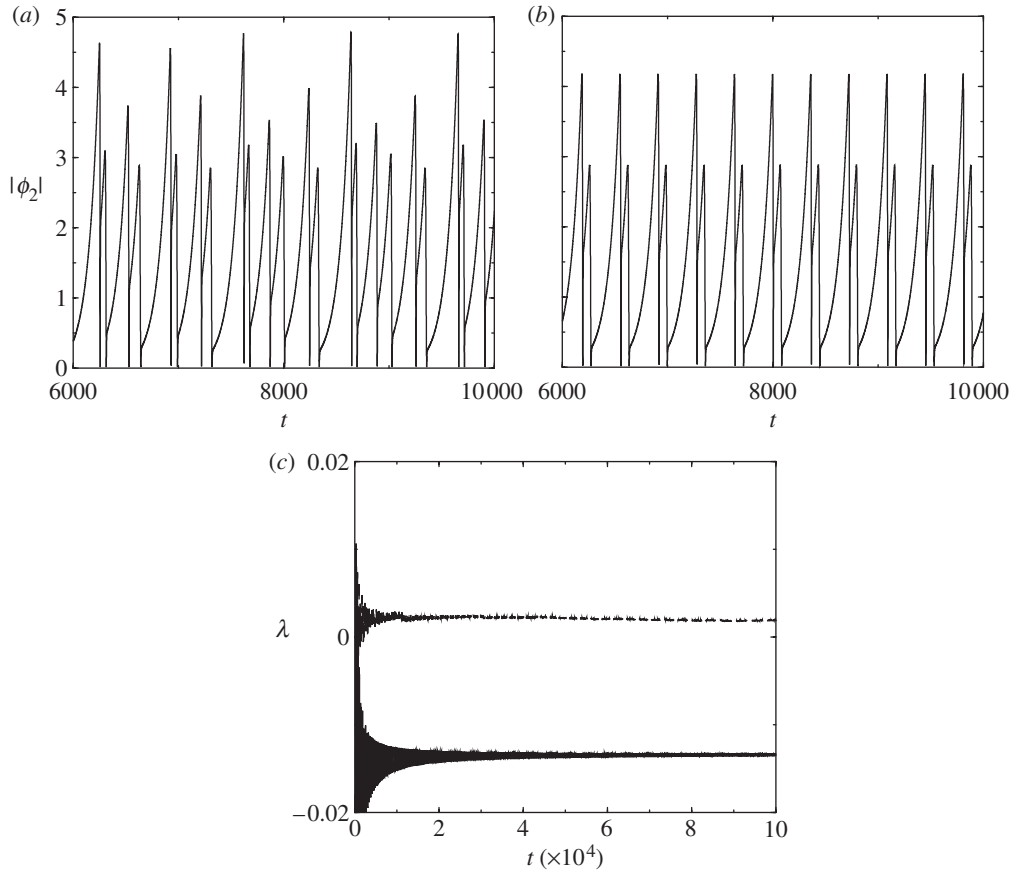


Figure 2. Time series for  $\gamma_2=0.01$ ,  $\gamma_1=\gamma_3=-0.194$  and (a)  $\epsilon=0$ , (b)  $\epsilon=10^{-10}$ , (c) maximal Lyapunov exponents for the cases (a,b).

The time series corresponding to the evolution of the pump wave amplitude  $|\phi_2(t)|$  with chaotic (uncontrolled) and periodic (controlled) attractors are shown in figure 2a,b, respectively. The overall behaviour of the pump wave is the same in both cases, since  $\phi_2$ , having a positive growth rate, initially increases exponentially at the linear rate  $\gamma_2$ , because the other modes (not shown) have small amplitudes. However, as they increase, the quadratic terms in (3.3)–(3.5) become significant and saturate the linear growth of the pump wave, causing its abrupt decay. The pump wave then imparts its energy to the daughter waves, which rapidly increase their amplitudes in spike-like events. Similarly, since the time-evolution of the daughter waves follows similar equations, their growth is also saturated by the nonlinear terms, and they also decay very fast, while the pump wave amplitude rises again completing the cycle.

In a chaotic situation (figure 2a), the time intervals between consecutive maxima of the pump wave amplitude vary in an irregular fashion, as well as the values taken on by these maxima. On the other hand, for periodic behaviour (figure 2b), the time intervals and the maximum amplitudes repeat themselves with a well-defined periodicity. Figure 2c shows the time evolution of the maximal Lyapunov exponent for both cases, confirming the chaoticity of the uncontrolled dynamics.

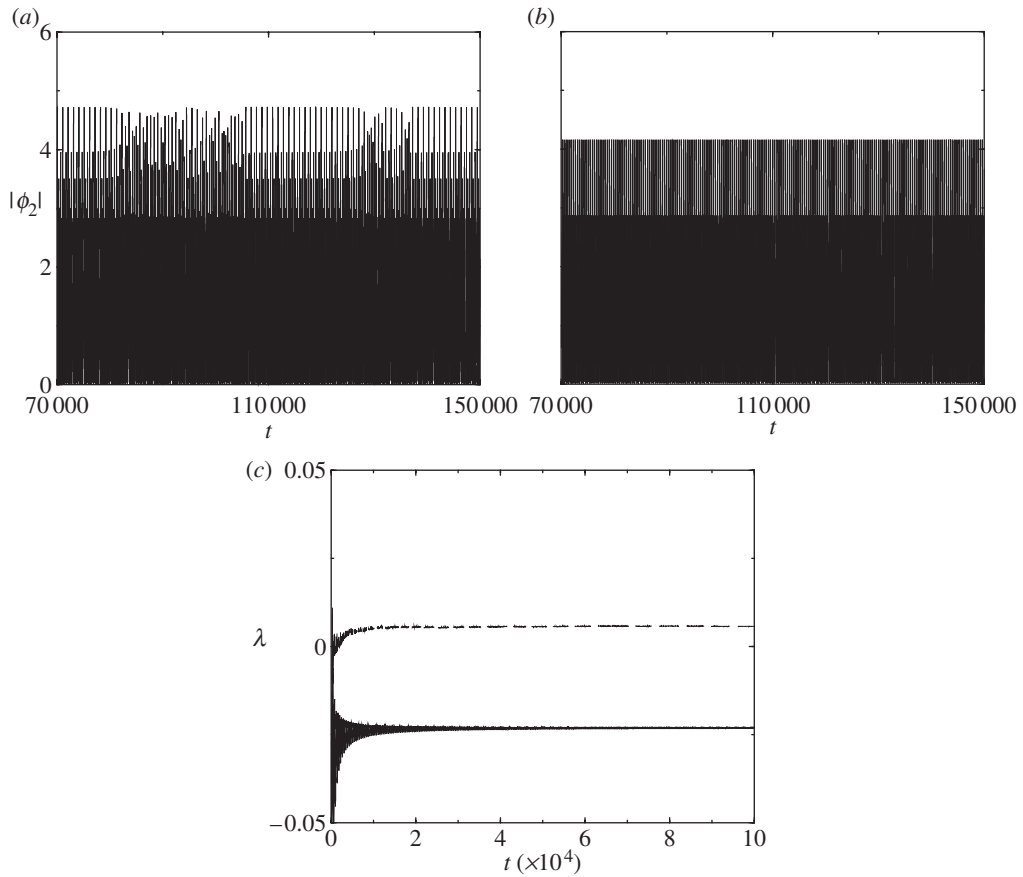


Figure 3. Time series for  $\gamma_2=0.01$ ,  $\gamma_1=\gamma_3=-0.19266$  and (a)  $\epsilon=0$ , (b)  $\epsilon=10^{-10}$ , (c) maximal Lyapunov exponents for the cases (a,b).

Besides the control of chaotic time series, the introduction of a fourth resonant wave of small amplitude can also suppress the intermittent switching between laminar regions of periodic motion and chaotic bursts, which happens for certain parameter values (Batista *et al.* 2006). Figure 3a shows an example of such behaviour for the uncontrolled system, which is suppressed for  $\epsilon=10^{-10}$  (figure 3b), as confirmed by the corresponding maximal Lyapunov exponents (figure 3c).

The preceding results refer to interacting modes in the Fourier space, but we can describe our resonant control procedure also in the configuration space, by focusing on a given point, say  $x=y=0$ , and considering the superposition of the three modes in (2.3). The evolution of the (dimensionalized) drift-wave potential is shown by figure 4a during a time interval of 0.6 ms, for the same parameters as in figure 2a, i.e. without control. This time series exhibits the same range of values as in typical measurements of the floating potential in small tokamaks (Castro *et al.* 1996). The application of a resonant perturbation of strength  $\epsilon=10^{-10}$ , while keeping the signal within the same range, presents a clear increase in the periodicity content (figure 4b).

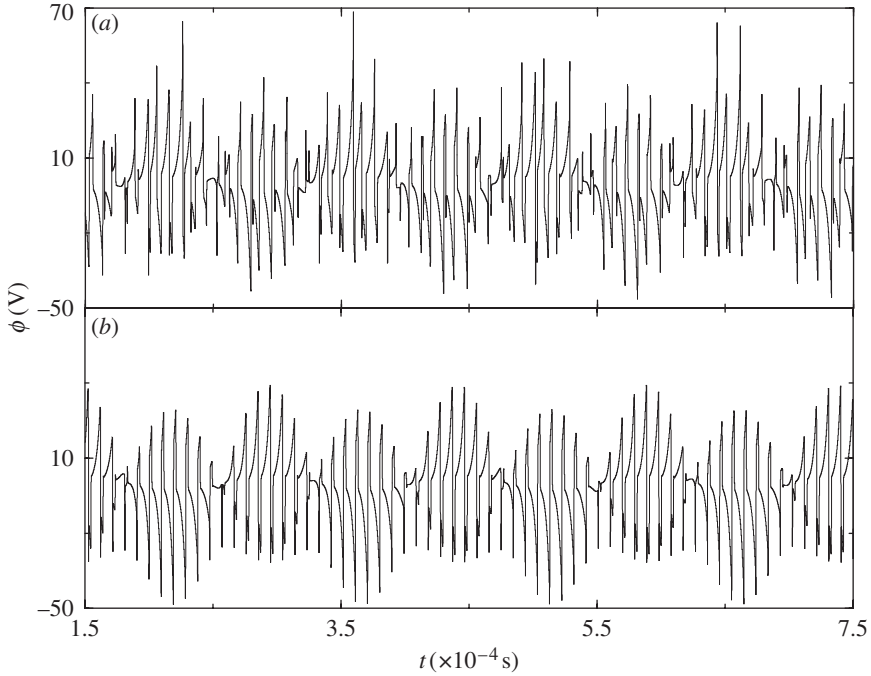


Figure 4. Time evolution of the drift-wave potential (in dimensional variables) for  $\gamma_2=0.01$ ,  $\gamma_1=\gamma_3=-0.194$  and (a)  $\epsilon=0$ , (b)  $\epsilon=10^{-10}$ .

The dependence of the dynamics on the control parameter  $\gamma_1$  is illustrated by the bifurcation diagram shown in figure 5, in which we plot the asymptotic values of  $\max|\phi_2|$  versus the strength of the resonant perturbation  $\epsilon$ , the remaining parameters being held constant. This form of sampling yields results qualitatively similar to a stroboscopic Poincaré map and furnishes valuable information on the system dynamics (Batista *et al.* 2006). As a general trend, an increase in  $\epsilon$  leads to a less complex dynamics, starting from a two-band chaotic attractor for the uncontrolled dynamics, and evolving, through an inverse period-doubling cascade, towards low-period orbits. In this way we can, at least in principle, choose the amplitude of the control wave to be applied in order to steer the chaotic trajectory to some desired low-period stable orbit, which may be a stationary state of interest, from the point of view of controlling drift-wave turbulence in the plasma edge.

We also considered the effect of the control on the bifurcation diagram obtained when the parameter  $\gamma_1$  is varied. Figure 6a shows such a diagram for the uncontrolled system ( $\epsilon=0$ ), which has been analysed in a previous work (Batista *et al.* 2006). The worth-mentioning aspect of this figure is the relative prevalence of chaotic dynamics for  $\gamma_1$  higher (in absolute value) than  $\approx 0.2$ , appearing due to a period-doubling cascade. If a weak-amplitude perturbation is applied (figure 6b), there follows that this chaotic region is substantially reduced in size, and it terminates through other period-doubling cascades, characterizing a bifurcation *bubble* for which a stable period-two orbit lies in the formerly chaotic region. A bifurcation bubble is the combination, in the bifurcation

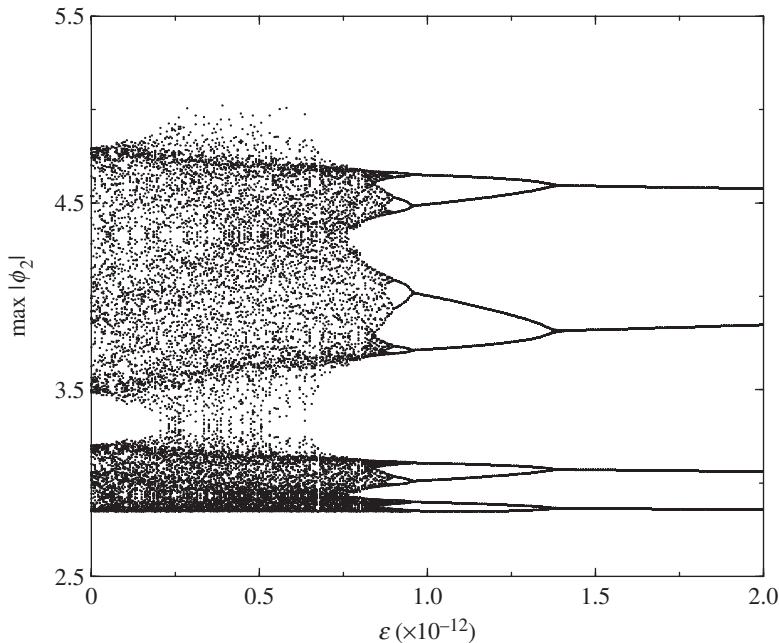


Figure 5. Bifurcation diagram for  $\max|\phi_2|$  versus the strength of the resonant perturbation  $\epsilon$ , for  $\gamma_2=0.01$ ,  $\gamma_1=\gamma_3=-0.194$ .

diagram of a given dynamical system, of a period-doubling cascade starting from a stable fixed point and leading to chaos, followed by an inverse, or period-halving cascade leading eventually to a single fixed point. This effect is even more visible for higher  $\epsilon$  (figure 6c), since the bubble terminates in a period-one orbit at  $\gamma_1 \approx -0.36$ .

#### 4. Conclusions

In this work we investigated the application of a control procedure in a low-dimensional dynamical system which is a truncated Fourier-mode expansion stemming from the high-dimensional problem of drift-wave turbulence in the plasma edge of a tokamak. We used an additional resonant perturbation of weak amplitude, and we showed that this strategy can stabilize chaotic orbits with very small control amplitudes, which turns to be an interesting feature from the experimental perspective. Many cautionary remarks are in order, though.

The first one is that our control strategy is a suppression of chaos scheme rather than a control procedure in the sense of the Ott–Grebogi–Yorke method, for example (Shinbrot *et al.* 1993). In the latter, one adjusts an external perturbation strength to steer the chaotic trajectory into the stable manifold of a desired unstable periodic orbit embedded in the chaotic attractor, by following the chaotic trajectory until it comes close enough to the unstable orbit one wishes to stabilize. By way of contrast, in our control procedure we used a resonant perturbation which may be viewed of as coming from the modes not included in the three-mode truncation. In this sense, our perturbation is intrinsic to the

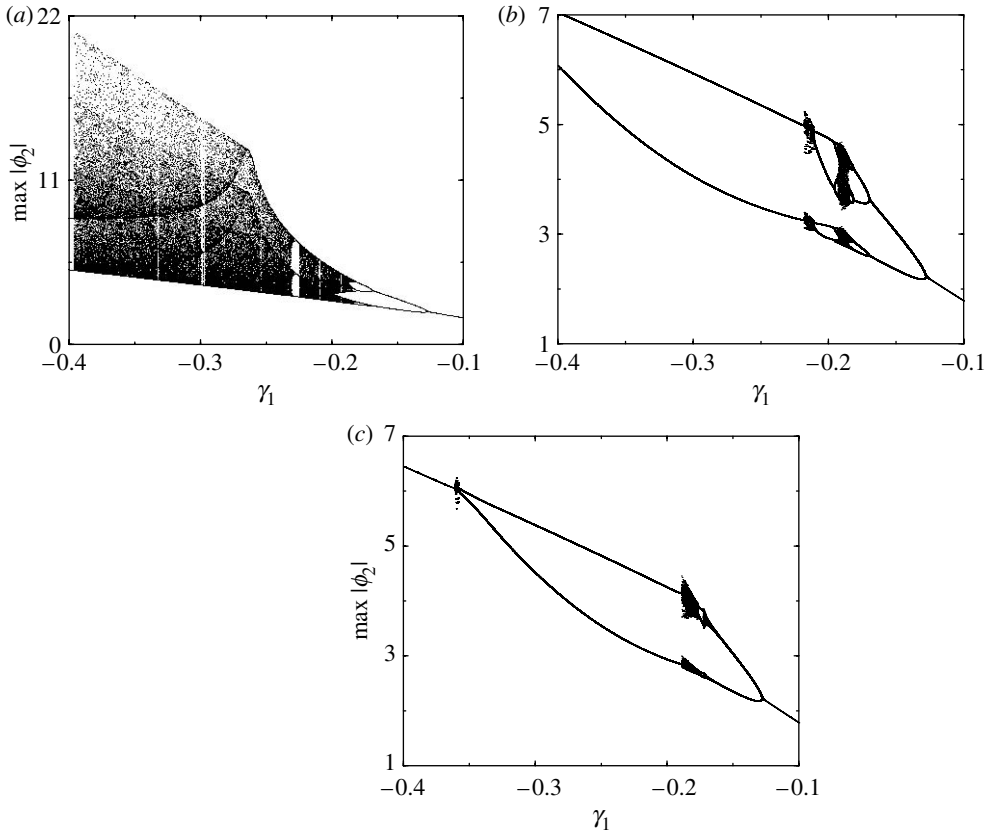


Figure 6. Bifurcation diagrams for  $\max|\phi_2|$  versus  $\gamma_1$ , for  $\gamma_2=0.01$  and (a)  $\epsilon=0.0$ , (b)  $\epsilon=10^{-12}$ , (c)  $\epsilon=10^{-10}$ .

system, and cannot be easily adjusted so as to choose a low-period orbit for the controlled dynamics. Moreover, since the wave perturbation is resonant with the other three waves, its strength can be very small, with the same order of magnitude as the environmental noise, for example.

As a result, we cannot choose *a priori* to what periodic orbit the system will converge asymptotically, but we have shown that chaos suppression is possible by means of intrinsic resonances with small amplitudes. We have restricted our description to three Fourier modes, and considered the control wave as a resonant fourth mode. In principle, a comprehensive description of drift-wave turbulence would involve a very large (in fact infinite) number of such modes. However, other modes are included in such a way that a multiplet is formed by sets of triplets. Hence, one can regard a wave triplet as a kind of building block of the processes involved in large-scale turbulence, and the understanding of its control mechanisms may shed some light on future spatio-temporal control procedures.

This work was partially supported by CNPq (Brazilian Government Agency), FAPESP (São Paulo State Agency). We acknowledge Dr W. Horton and Dr P.J. Morrison (Institute for Fusion Studies, University of Texas) for their valuable suggestions.

## References

- Batista, A. M., Caldas, I. L., Lopes, S. R., Viana, R. L., Horton, W. & Morrison, P. J. 2006 Nonlinear three-mode interaction and drift wave turbulence in a tokamak edge plasma. *Phys. Plasmas* **13**, 042510:1–042510:10. (doi:10.1063/1.2184291)
- Castro, R. M., Heller, M. V. A. P., Caldas, I. L., da Silva, R. P., Brasílio, Z. A. & Nascimento, I. C. 1996 Temperature fluctuations and plasma edge turbulence in the Brazilian tokamak TBR. *Phys. Plasmas* **3**, 971–977. (doi:10.1063/1.871802)
- Chian, A. C.-L., Lopes, S. R. & Alves, M. V. 1994 Generation of auroral whistler-mode radiation via nonlinear coupling of Langmuir waves and Alfvén waves. *Astron. Astrophys.* **290**, L13–L16.
- Hasegawa, A. & Mima, K. 1977 Stationary spectrum of strong turbulence in magnetized nonuniform plasma. *Phys. Rev. Lett.* **39**, 205–208. (doi:10.1103/PhysRevLett.39.205)
- Hasegawa, A. & Mima, K. 1978 Pseudo-three-dimensional turbulence in magnetized nonuniform plasma. *Phys. Fluids* **21**, 87–92. (doi:10.1063/1.862083)
- Hasegawa, A., MacLennan, C. G. & Kodama, Y. 1979 Nonlinear behaviour and turbulence spectra of drift waves and Rossby waves. *Phys. Fluids* **22**, 2122–2129. (doi:10.1063/1.862504)
- Heller, M. V. A. P., Castro, R. M., Caldas, I. L., Brasílio, Z. A., da Silva, R. P. & Nascimento, I. C. 1997 Correlation between plasma edge electrostatic and magnetic oscillations in the Brazilian tokamak TBR. *J. Phys. Soc. Jpn* **66**, 3453–3460. (doi:10.1143/JPSJ.66.3453)
- Horton, W. & Hasegawa, A. 1994 Quasi-two-dimensional dynamics of plasmas and fluids. *Chaos* **4**, 227–251. (doi:10.1063/1.166049)
- Horton, W. 1999 Drift waves and transport. *Rev. Mod. Phys.* **71**, 735–778. (doi:10.1103/RevModPhys.71.735)
- Hu, G. & He, K. 1993 Controlling chaos in systems described by partial differential equations. *Phys. Rev. Lett.* **71**, 3794–3797. (doi:10.1103/PhysRevLett.71.432)
- Karplyuk, K. S., Oraevskii, V. N. & Pavlenko, V. P. 1973 Dynamics of the non-linear interaction of magnetohydrodynamic waves. *Plasma Phys.* **15**, 113–124. (doi:10.1088/0032-1028/15/2/005)
- Katou, K. 1982 Resonant three-wave interaction in electrostatic drift-wave turbulence. *J. Phys. Soc. Jpn* **51**, 996–1000. (doi:10.1143/JPSJ.51.996)
- Lopes, S. R. & Chian, A. C.-L. 1996 Controlling chaos in nonlinear three-wave coupling. *Phys. Rev. E* **54**, 170–174. (doi:10.1103/PhysRevE.54.170)
- Shinbrot, T., Grebogi, C., Yorke, J. A. & Ott, E. 1993 Using small perturbations to control chaos. *Nature* **363**, 411–417. (doi:10.1038/363411a0)
- Terry, P. & Horton, W. 1982 Stochasticity and the random phase approximation for three electron drift waves. *Phys. Fluids* **25**, 491–501. (doi:10.1063/1.863761)
- Terry, P. & Horton, W. 1983 Drift wave turbulence in a low-order k space. *Phys. Fluids* **26**, 106–112. (doi:10.1063/1.863997)
- Wagner, F. & Stroth, U. 1993 Transport in toroidal devices—the experimentalist’s view. *Plasma Phys. Control. Fusion* **35**, 1321–1371. (doi:10.1088/0741-3335/35/10/002)
- Walters, D. & Lewak, G. J. 1977 Dynamics of four coupled plasma waves to second order. *J. Plasma Phys.* **18**, 525–536.